2722
→ public

Modal power decomposition of beam intensity profiles into LP modes of multimode optical fibers

Daniel Beom Soo Soh*, Johan Nilsson, Seungin Baek, Christophe Codemard,
Yoonchan Jeong, Valery Philippov
Optoelectronics Research Centre, University of Southampton, Southampton, SO17 1BJ, UK
* Corresponding author, e-mail: dbs@orc.soton.ac.uk, tel: +44-23-8059-3143, fax: +44-23-8059-3142

Abstract

We calculate the modal power distribution of a randomly polarized LP multimode beam inside a cylindrical fiber core from knowledge of spatial intensity profiles of a beam emitted from the fiber. We provide an exact analysis with rigorous proofs that forms the basis for our calculations. The beam from the fiber end is collimated by a spherical lens with a specific focal length. The original LP mode basis is transformed by the spherical lens and forms another orthogonal basis that describes the free space beam. Using this, the modal power distribution is calculated from the mutual intensity profile. This was acquired by adopting a well-known mutual intensity profile retrieving technique, based on measurements of the intensity patterns several times after two perpendicular cylindrical lenses with varying separation. Feasibility of our decomposition algorithm is demonstrated with simulations.

OCIS codes: (060.2310) Fiber Optics, (030.4070) Modes

1. INTRODUCTION

Modal decomposition of light beams in multimode optical fibers is a key problem in various areas such as optical fiber communications and optical fiber lasers. For instance, knowledge of the power distribution among modes is necessary in applications such as higher order mode dispersion compensation, mode beating devices, and free space optical communication employing fiber lasers and amplifiers. Moreover, novel multimode fiber devices such as cladding-pumped fiber lasers[1-3] require a thorough knowledge and analysis of the modal behavior of launched beams, for example, in order to optimize the optical pumping scheme. Approximate methods for multimode fibers which assumed that the modal space is continuous or the modal fields are azimuthally symmetric were developed in the 1980's[4-8], but to date there has not been an exact analytical treatment of modal decomposition of beams in optical fibers based on intensity profile measurements.

Recently, a Hermite-Gaussian modal decomposition was demonstrated by Gori and Santarsiero, et. al.[9,10], who successfully decomposed a multimode Hermite-Gaussian beam into eigenmodes and determined the modal power weights. One advantage of the Hermite-Gaussian beam is the orthogonality properties of the Fourier-transformed modal intensity functionals[9]. This makes the method feasible and calculable. Unfortunately, the LP mode intensity profiles of an optical fiber are more difficult to treat, because of the complicated nature of the Bessel solutions of the Helmholtz equation with a cylindrical boundary. While one can easily extract modal weights from the complex field profiles, thanks to the orthogonality of the Helmholtz solutions, this requires knowledge of the phase profile of the beam as well as the amplitude. In practice, interferometric measurements have been used to determine the shape of the wavefronts[11-12]. Alternatively one can use optimizing iterative methods with least square fitting[13]. However, both of these methods have problems. For instance, the temporal coherence of light sources may be insufficient for interferometric measurements while iterative methods are often cumbersome.

In this paper, we present a concise method for determining the modal power weights of a beam in a multimode fiber from intensity measurements. Our method allows the modal power weights to be calculated from these simple intensity measurements without loss of accuracy. We first review modal properties and beam propagation in multimode fibers. Then our proposed decomposition method is described in a mathematically rigorous way. We finally present realistic simulation results obtained with a numerical implementation of our method.

2. MODAL PROPERTIES REVIEW

For completeness we here briefly review some of the modal properties of optical fibers.

Consider a step index fiber with an assumption of weak guiding. Then, the electrical field of the beam inside the core can be assumed to be in the form of

$$\bar{E}(x,y,z)=\bar{e}(x,y)\exp(i\beta z), \tag{1}$$

where x, y, z denote the Cartesian coordinates of a point and β is propagation constant in the direction of the Z-axis. The representation in (1) is an eigenmode of the fiber, while the general field can be expressed as a superposition of weighted eigenmodes. It is noted that the electrical field distribution $\vec{e}$ does not change along the Z-axis in (1). This comes from that we consider only bound beams, which are in a spatially steady state. Moreover, we assume that the electrical field is perpendicular to the Z-axis because of the weakly guiding assumption. The electrical field $\vec{e}$ is a solution of the paraxial equation

$$\left\{\nabla_t^2 + k^2 n(r)^2 - \beta^2\right\}\vec{e}(x, y) = 0, \tag{2}$$

where ∇_t^2 denotes the transverse Laplacian ($= \partial^2/\partial x^2 + \partial^2/\partial y^2$), $k = 2\pi/\lambda$, λ is the free space wavelength of the beam, and $n(r)$ is the index profile of the fiber. Assume we have the core boundary at radius ρ and normalize the radial variable r as $R \overset{\Delta}{=} r/\rho$. Then,

$$n(R) = \begin{cases} n_{co}, \text{if } 0 \le R \le 1 \\ n_{cl}, \text{if } 1 < \mathrm{R} \end{cases}, \tag{3}$$

where n_{co} denotes the core refractive index, n_{cl} the cladding refractive index and $n_{co} > n_{cl}$. For simplicity we consider a step-index core.

It is well known that the solutions of (2) take the approximated form of linearly-polarized (LP) modes[14]

$$\vec{e}^{\,lpij}(x, y) = F_{lp}(R)\left\{\sin\left(l\phi + \frac{\pi}{2}i\right)\hat{x} + \sin\left(l\phi + \frac{\pi}{2}j\right)\hat{y}\right\}, \tag{4}$$

where $i, j = 0,1$ and $\hat{x}$, $\hat{y}$ denote unit vectors in the direction of X-axis and Y-axis, respectively. Here, F_{lp} is a solution of

$$\left\{\frac{d^2}{dR^2} + \frac{1}{R}\frac{d}{dR} + k^2 n^2 - \frac{l^2}{R^2} - \beta^2\right\} F_{lp}(R) = 0\,. \qquad (5)$$

Note that there are two polarization states in each LP mode, namely the x- and y-polarized states. These two sets of polarizations are mutually perpendicular in space. Hence, we can consider only one polarization at a time without loss of generality. In other words, we can consider the solution set as $\vec{e}_t^{\,lpij} = e_t^{lpi}\hat{x} + e_t^{lpj}\hat{y}$, and $e_t^{lpi}(x,y) = F_{lp}(x,y)\sin(l\phi + i\pi/2)$. We denote e_t^{lp0} as sine-modes and e_t^{lp1} as cosine-modes. Each modal solution has sine- and cosine-modes unless $l = 0$. For $l = 0$, the modal solution does not depend on ϕ, thus, it is an even function with respect to ϕ. Because of this, we still call the modal solutions of $l = 0$ as cosine modes.

The solutions of (5) are given by

$$F_{lp}(R) = \begin{cases} J_l(U_{lp}R)/J_l(U_{lp}), & 0 \le R < 1 \\ K_l(W_{lp}R)/K_l(W_{lp}), & \text{otherwise} \end{cases}, \qquad (6)$$

where $U_{lp} \overset{\Delta}{=} \rho\sqrt{k^2 n_{co}^2 - \beta_{lp}^2}$, $W_{lp} \overset{\Delta}{=} \rho\sqrt{\beta_{lp}^2 - k^2 n_{cl}^2}$. For a given l, $(l = 0,1,2,\cdots)$, the U_{lp}'s and W_{lp}'s ($p = 1,2,3,\cdots$) are all the possible solutions satisfying the boundary condition

$$U_{lp}\frac{J_{l+1}(U_p)}{J_l(U_p)} = W_{lp}\frac{K_{l+1}(W_p)}{K_l(W_p)}\,. \qquad (7)$$

It follows that the propagation constants β_{lp} are different for different modes. In (7), it is well known that the number of possible U_{lp}'s and W_{lp}'s are finite for given finite physical dimensions of a fiber. Hence, we have maximum numbers of both l and p for given physical dimension of the fiber such that $0 \le l \le l_0$, $1 \le p \le p_0(l)$ – the maximum number p_0 is a function of l, which can be seen from (7). This in turn means that the number of modes for given fiber physical dimension is finite.

Now, define the mode set Ω as the set of e^{lpi} such that each U_{lp}, W_{lp} associated with F_{lp} satisfy the boundary condition (7). Any linear combination of members of Ω is also a solution of (2). Hence, the solution functional space is a span of Ω. In fact, it is a subset of the space of squarely integrable functions in L_2. With a properly defined inner product, Ω forms the basis of a Hilbert space. For this, we define an inner product as $\langle e_i, e_j \rangle \overset{\Delta}{=} \int_{-\infty}^{\infty}\int_{-\infty}^{\infty} e_i(x,y) e_j^*(x,y)\,dxdy$, where e_i, e_j are members of the solution functional space and the star (*) denotes the complex conjugate. It is also possible to define the induced norm of the functional space by $\left\| e^{lpi} \right\| = \sqrt{\langle e^{lpi}, e^{lpi} \rangle}$.

The basis of the solution functional space can be chosen as a set of orthogonal solutions of Maxwell's equations. The modes are a good candidate for the maximal orthogonal set, i.e., the basis for the solution functional space. It is easy to prove that all the modes are orthogonal and moreover, the set Ω is the maximal orthogonal set. (Appendix A.)

Now, it is possible to construct the orthonormal basis with $\overline{\Omega} = \left\{ \overline{e}^{lpi} \middle| \overline{e}^{lpi} = e^{lpi} / \left\| e^{lpi} \right\| \right\}$. For convenience, we reorder the (l, p, i) modes into modes with one index n, ($n = 1,2,3,\cdots,N$; N is the number of eigenmodes), which is possible since there is a one-to-one, onto mapping from a finite l_3 space to a finite l_1 space. In other words, $\overline{\Omega} = \left\{ \overline{e}^{n} \middle| \overline{e}^{n} = e^{n} / \left\| e^{n} \right\| \right\}$. Then, by Hilbert space theory and by the completeness of the L_2 space, any solution of the Maxwell equation in (2) can be expressed as a linear combination of members in $\overline{\Omega}$ on a complex scalar field:

$$e = \sum_{i=1}^{N} c_i \overline{e}^{\,i} . \tag{8}$$

Here, if we consider a partially coherent beam, the c_i's are ensemble averaged values of a set of partially coherent beams, i.e., $c_i = \langle c_i \rangle$. It is noteworthy that the c_i's are also complex values because each mode might have different phase. The power is given by $P = \|e\|^2 / \eta$, where η denotes the impedance in the fiber. Then, by orthogonality, it easily follows that

$$P = \frac{1}{\eta} \sum_{n=1}^{N} |c_i|^2 , \tag{9}$$

because each eigenmode power is given by $\left\| \overline{e}^{\,i} \right\|^2 / \eta = 1/\eta$. Hence, from (9) we know that the total power is a linear sum of each modal weight $|c_i|^2$ divided by the impedance.

3. MODAL POWER DISTRIBUTION

If we know the amplitude and phase of the electrical field e, it is straightforward to evaluate the c_i's by simple inner product

$$c_i = \langle e, \bar{e}^i \rangle = \int_{-\infty}^{\infty}\int_{-\infty}^{\infty} e(x,y)\bar{e}^{i*}(x,y)dxdy. \tag{10}$$

The electrical field e with knowledge of phase is difficult to determine while the intensity profile $|e|^2$ can be easily obtained with a camera. We propose to calculate the modal power weights $|c_i|^2$ from the mutual intensity profile or two-point correlation function defined as[15]

$$\Gamma(x_1, y_1; x_2, y_2) \overset{\Delta}{=} e(x_1, y_1)e^*(x_2, y_2). \tag{11}$$

The mutual intensity profile can be evaluated from measurements of intensity profiles with a camera. Assuming then that the mutual intensity profile at some point in the fiber and all the modes are known, $|c_i|^2$ are calculated as follows. Note that

$$\int_{-\infty}^{\infty}\int_{-\infty}^{\infty} \Gamma(x_1, y_1; x_2, y_2)\bar{e}^i(x_2, y_2)dx_2dy_2 = c_i e(x_1, y_1). \tag{12}$$

The above equation is an integral equation and generally not solvable. However, if we take the complex conjugate of (12) and multiply this to (12) and integrate with respect to x_1, y_1, we get

$$|c_i|^2 \int_{-\infty}^{\infty}\int_{-\infty}^{\infty} e(x,y)e^*(x,y)dxdy = \int_{-\infty}^{\infty}\int_{-\infty}^{\infty} \left| \int_{-\infty}^{\infty}\int_{-\infty}^{\infty} \Gamma(x_1, y_1; x_2, y_2)\bar{e}^i(x_2, y_2)dx_2dy_2 \right|^2 dx_1dy_1. \tag{13}$$

According to Parseval's theorem for a Hilbert functional space with orthonormal basis, we have that

$$\int_{-\infty}^{\infty}\int_{-\infty}^{\infty}|e(x,y)|^2 dxdy = \sum_{n=1}^{N}|c_n|^2 . \tag{14}$$

Now, summing both left and right hands in (13) with respect to index i , and employing (14) give

$$|c_i|^2 = \Lambda_i / \sqrt{\sum_{n=1}^{N}\Lambda_n} , \tag{15}$$

where

$$\Lambda_i = \int_{-\infty}^{\infty}\int_{-\infty}^{\infty}\left|\int_{-\infty}^{\infty}\int_{-\infty}^{\infty}\Gamma(x_1,y_1;x_2,y_2)\bar{e}^{i}(x_2,y_2)dx_2dy_2\right|^2 dx_1dy_1 . \tag{16}$$

Thus, once the mutual intensity profile is known, the modal power weights can be calculated. A necessary condition is that all the mode profiles must be known. On the other hand, there is no assumption about the shape of the waveguide or the modes.

The method requires that the mutual intensity profile of the beam is determined. It is difficult to evaluate the beam properties inside the fiber. Here, we suggest to use an alternative method to evaluate the $|c_i|$'s, at the exit of the fiber, with the setup shown in Fig. 1. We first collimate the beam from the fiber end using a spherical lens with appropriate focal length f. Then, the $|c_i|$'s can be calculated by considering the orthogonal functionals in the free space, as follows..

It follows from the weakly guiding approximation that a paraxial treatment can be adopted[13]. Hence, using Fourier optics and with reference to Fig. 1, the electrical field $e(x_1, y_1; z=-f)$ at the $z=-f$ plane and the electrical field $e(x_2, y_2; z=d)$ at the $z=d(>0)$ plane are related to each other by a Fourier transform multiplied by a phase term[14];

$$e(x_1, y_1; z=-f) = \frac{1}{-j\lambda f} e^{-j\frac{k}{2f}(x_1^2+y_1^2)\left(1-\frac{d}{f}\right)} \int_{-\infty}^{\infty}\int_{-\infty}^{\infty} e(x_1', y_1'; z=d) e^{-j\frac{k}{f}(x_1x_1'+y_1y_1')} dx_1'dy_1', \qquad (17)$$

where f is the focal length of the spherical lens, and $k = 2\pi/\lambda$ the free space propagation constant. It is noted that the inverse mapping from $e(x_1, y_1; z=d)$ to $e(x_1, y_1; z=-f)$ depends on the distance d because of the phase term in the right hand side of (17), i.e. $-jk(x_1^2+y_1^2)(1-d/f)/2f$. Physically, it means that the wavefronts of the free space beam change according to the distance from the lens. However, with an appropriate focal length the phase term becomes negligible over a distance range of interest, which is much larger than the focal length: Choose f such that $k(x_1^2+y_1^2)(1-d/f)/2f \cong k(x_1^2+y_1^2)d/2f^2 << 1$, that is

$$\rho\sqrt{kd_M} << f << d_m, \qquad (18)$$

where ρ is the fiber core radius and it is assumed that the distance of interest is in the range $d_m < d < d_M$. Then, the phase term in (17) can be ignored so that the approximation holds as follows.

$$e(x_1, y_1; z=-f) \cong \frac{1}{-j\lambda f} \int_{-\infty}^{\infty}\int_{-\infty}^{\infty} e(x_1', y_1'; z=d) e^{-j\frac{k}{f}(x_1x_1'+y_1y_1')} dx_1'dy_1'. \qquad (19)$$

Since the inverse mapping from $e(x_1, y_1; z = d)$ to $e(x_1, y_1; z = -f)$ does not depend on d any more, it holds that

$$\tilde{e}(x, y)\left(\overset{\Delta}{=} e(x, y; z = f)\right) \cong e(x, y; z = d), \quad \forall d, \;\; f < d < f^2 / \rho^2 k, \tag{20}$$

provided the beam propagates in an isotropic medium such as air.

Next step is to consider the orthogonal functional basis set in free space. It is easily shown that the LP mode fields Fourier transformed as in (19) form also an orthogonal basis for the free space beam, by using Parseval's theorem as follows. We define the transformed LP mode $\bar{e}_F^i$ as

$$\bar{e}_F^i(x, y) = \frac{1}{-j\lambda f}\int_{-\infty}^{\infty}\int_{-\infty}^{\infty} \bar{e}^i(x', y'; z = -f) e^{j\frac{k}{f}(xx' + yy')} dx' dy'. \tag{21}$$

Note that this is the inverse transform of (19). Now the general Parseval's theorem has that

$$\begin{aligned}
\left\langle \bar{e}_F^i, \bar{e}_F^j \right\rangle &= \int_{-\infty}^{\infty}\int_{-\infty}^{\infty} \bar{e}_F^i(x, y)\bar{e}_F^{j*}(x, y) dx dy \\
&= \frac{1}{\lambda^2 f^2}\int_{-\infty}^{\infty}\int_{-\infty}^{\infty}\int_{-\infty}^{\infty}\int_{-\infty}^{\infty}\int_{-\infty}^{\infty}\int_{-\infty}^{\infty} \bar{e}^i(x', y')\bar{e}^{j*}(x'', y'') e^{j\frac{k}{f}(x(x'-x'')+y(y'-y''))} dx' dy' dx'' dy'' dx dy \\
&= \frac{1}{\lambda^2 f^2}\int_{-\infty}^{\infty}\int_{-\infty}^{\infty}\int_{-\infty}^{\infty}\int_{-\infty}^{\infty} \bar{e}^i(x', y')\bar{e}^{j*}(x'', y'')\delta(x'-x'')\delta(y'-y'')\lambda^2 f^2 dx' dy' dx'' dy'' \\
&= \int_{-\infty}^{\infty}\int_{-\infty}^{\infty} \bar{e}^i(x'', y'')\bar{e}^{j*}(x'', y'') dx'' dy'' \\
&= \left\langle \bar{e}^i, \bar{e}^j \right\rangle.
\end{aligned} \tag{22}$$

Hence, it is shown that the $\bar{e}_F^i$'s are also an orthonormal set. Then, Fourier-transforming (8) gives together with (21) that

$$\tilde{e}(x,y)=\sum_{i=1}^{N} c_i \bar{e}_F^i . \tag{23}$$

with the same expansion coefficients, i.e., modal weight c_i's. Since $\bar{e}_F^i$'s are also orthonormal, the derivation from (11) - (16) can be similarly applied giving a series of equations

$$\Gamma_F(x_1,y_1;x_2,y_2)\overset{\Delta}{=}\tilde{e}(x_1,y_1)\tilde{e}^*(x_2,y_2), \tag{24}$$

$$\int_{-\infty}^{\infty}\int_{-\infty}^{\infty}\Gamma_F(x_1,y_1;x_2,y_2)\bar{e}_F^i(x_2,y_2)dx_2dy_2 = c_i\tilde{e}(x_1,y_1), \tag{25}$$

and, hence,

$$|c_i|^2 = \Lambda_F^i \Big/ \sqrt{\sum_{n=1}^{N}\Lambda_F^n} , \tag{26}$$

where

$$\Lambda_F^i = \int_{-\infty}^{\infty}\int_{-\infty}^{\infty}\left|\int_{-\infty}^{\infty}\int_{-\infty}^{\infty}\Gamma_F(x_1,y_1;x_2,y_2)\bar{e}_F^i(x_2,y_2)dx_2dy_2\right|^2 dx_1dy_1 . \tag{27}$$

Thus, we can calculate the original modal weights $\left|c^i\right|^2$ by employing the new orthonormal basis e_F^i's in free space. If one can get the e^i's by solving (2), it is easy to get the e_F^i's via a Fourier transform (21). Now, it still remains to get the mutual intensity profile of the free space beam.

Methods for obtaining the mutual intensity profile of a beam by measuring only the intensity patterns have been studied recently. For instance, it is possible to retrieve the mutual intensity profile using the Wigner function combined with the Radon transform[16-18], or using the

AF function combined with the Radon transform[19]. Here, one can choose either of the methods and, in our case, the Wigner function method in ref. 17 is adopted for the purpose of numerical simulations. The Wigner function method is based on using two cylindrical lenses and spatially resolved intensity measurements, e.g., with a CCD camera. One thing to note with mutual intensity retrieval techniques is that it is assumed that the phase front of the beam should be reasonably flat against the propagation axis[17], which in our case is guaranteed by choosing an appropriate focal length of the spherical lens as in (18). The task to get the mutual intensity profile of the paraxial free space beam is well described in ref. 17, which is presented in Appendix B for readability.

To sum up, the modal decomposition is acquired by, first, getting the mutual intensity profile of the collimated beam after the spherical lens and, secondly, Fourier transforming each modal solution $\bar{e}^i$ by (21), and finally, calculating each modal coefficient with (26) and (27).

4. SIMULATIONS AND DISCUSSIONS

To show the feasibility of our proposed algorithm, we present a realistic simulation with realistic fiber parameters. We considered a step index fiber with core numerical aperture (NA)=0.2, core radius 4 μm, n_{cl}=1.457. We used a wavelength $\lambda = 977\,nm$. These parameters result in a normalized frequency V = 5.14, Using the boundary condition in (7), the modal number l, p's and the effective refractive index n_{eff} of the each mode with relationship $n_{eff}^{lp} = \beta_{lp}\lambda / 2\pi$ were calculated. There are five LP modes as listed in Table 1. Note that some modes are split into cosine- and sine-modes as in (4), depending on the value of i. Figure 2 shows the mode intensity profile of each pair of mode representations $\bar{e}^i(x,y)$ and $\bar{e}^i_F(x,y)$, calculated using (21).

In order to evaluate our algorithm, we simulated two cases. In one case the exact mutual intensity profile at $z = f$ is known (Simulation A). The other simulation includes retrieval of the mutual intensity using the method described in Appendix B (Simulation B). We assigned an arbitrary set of test modal power weights $|c_i|^2$ as in Table 1 to evaluate the accuracy of our algorithm. Figure 3 shows the intensity of the test multimode beam of concern. Assuming that the collimated free space beam propagates in free space according to the Fresnel integration in (17) and (B5), we could obtain the calculated CCD images taken at the $z = D$ plane for various values of θ, ϕ, defined in Appendix B. In order to realize the inverse Radon transform, used to calculate the modal power weights, we used 30 different uniformly distributed angles in the interval $[-\pi/2, \pi/2]$ for each θ, ϕ. Assuming the focal length of the cylindrical lenses are $20\ cm$, varying d_i from $0.87m$ to $1.24m$ $(i = 1, 2)$ and D from $1.2\ m$ to $2.0\ m$ gave the full coverage of the required angles θ, ϕ according to (24), which is similar to ref. 17. Hence, the distances d_m and d_M in (18) were $0.87\ m$ and $2\ m$, respectively, which gave the condition on the focal length f of the spherical lens as $1.4\ cm << f << 87\ cm$. From this, we chose the focal length f of the spherical lens as $11\ cm$.

Simulation A calculated the modal power weights $|c_i|^2$ using (24) - (27) assuming the exact mutual intensity profile at $z = f$ is known while Simulation B calculated the $|c_i|^2$'s using a mutual intensity profile Γ_F that was retrieved from the intensity pattern after two cylindrical lenses. In simulation B, using these intensity profiles, which are selectively shown in Fig. 4 for some values of θ, ϕ, we could calculate the Wigner function at the $z = 0$ plane using the inverse Radon transformation. From this Wigner function, the mutual intensity profile Γ_F was obtained through 2-dimensional inverse Fourier transform. Now, by applying (24)-(27), the modal power weights are calculated as shown in Table 1. Figure 6 shows the modal power distribution in percent of the total power of the multimode beam. The test modal power distribution and the calculated results from simulation A, B are shown.

We also show the comparison between the intensity profiles of the test multimode beam inside the fiber and the calculated reconstructed beam in Fig. 5. One should note that it is impossible to reconstruct the multimode image by using calculated $|c_i|$'s. For a full reconstruction, the phases must also be known. However, purely for demonstration purpose, we assumed that we know all the test modal weights are positive numbers with zero phase. The reconstruction through simulation A is almost exact while simulation B results in some discrepancy. In the simulations, we used 50 grid points along each of the X- and Y-axis, i.e., 2500 points for one image. The errors between the initially assigned modal weights and the calculated ones are within 0.5 % for Simulation A while that of Simulation B were within 10 %. This implies that our proposed method of calculating modal distribution is quite accurate provided the mutual intensity profile is known sufficiently well.

The main cause of the simulation errors in Simulation B was the limited position/angle grid resolution. Obviously, the finer grids with more grid points were used, the more accurate results we could get. For instance, the retrieval of the Wigner function from the CCD camera through the Radon transform depended on the number of angles while the retrieval of mutual intensity profile from the Wigner function with Fourier transform depended on the number of grid points. Considering that CCD images normally provide more than 256×256 data points, the accuracy might be quite satisfactory provided that limitations such as a nonlinear response are controlled. In addition, a larger number of angles can be used for more accurate results.

5. CONCLUSIONS

We proposed a method for power decomposition into LP-modes of an optical fiber based on free-space intensity measurements. We presented a rigorous analysis of the proposed algorithm, demonstrating orthogonality of functionals and invariance of orthogonal functionals through Fourier transform.

Results of two simulations are shown, one assuming the mutual intensity profile of the free space beam is exactly known and the other also covering the full process of retrieving the mutual intensity profile. Our simulation errors were less than 0.5% for the exactly known mutual intensity profile and less than 10% if the inexact mutual intensity profile retrieval process was included in the simulation. Hence, if a better retrieval method is adopted in terms of speed and exactness, better accuracy with less effort might be obtained.

The method demands only that the guided beam inside a waveguide must be linearly polarized, and can be readily applied to other waveguides structures provided all the modes are known and linearly polarized.

Acknowledgements

We acknowledge Professor Kyunghwan Oh of K-JIST for valuable discussions.

APPENDICES

A. Orthogonality of the solution functionals

Let us consider the inner product of two arbitrary modes,

$$\left\langle e_t^{lpi}, e_t^{mqj} \right\rangle = \int_0^{2\pi} \int_0^{\infty} F_{lp}(R) F_{mq}(R) \sin\left(l\phi + \frac{\pi}{2} i \right) \sin\left(m\phi + \frac{\pi}{2} j \right) R dR d\phi , \tag{A1}$$

where we changed the integral coordinate from Cartesian to polar. It is easy to see that only if $l = m$ and $i = j$, the inner product in (A1) can have nonzero value because of the sinusoidal term in the integrand.

Now, consider

$$\left\langle e_t^{lpi}, e_t^{lqi} \right\rangle = \int_0^{2\pi} \int_0^{\infty} F_{lp}(R) F_{lq}(R) \sin^2\left(l\phi + \frac{\pi}{2} i \right) R dR d\phi = \pi \int_0^{\infty} F_{lp}(R) F_{lq}(R) R dR . \tag{A2}$$

Note that there is no sine mode for $l = 0$, i.e. $i = 1$ when $l = 0$. Hence, (A2) is valid for any l. The orthogonality of the F_{lp}'s is proved by classical way by considering the differential equation in (5). Consider

$$\left\{ \frac{d^2}{dR^2} + \frac{1}{R}\frac{d}{dR} - \frac{l^2}{R^2} + U_p^2 - V^2 f_n(R) \right\} F_{lp}(R) = 0 , \tag{A3}$$

$$\left\{\frac{d^2}{dR^2}+\frac{1}{R}\frac{d}{dR}-\frac{l^2}{R^2}+U_q^2-V^2 f_n(R)\right\}F_{lq}(R)=0, \tag{A4}$$

where $f_n(R)=\begin{cases}0, \text{if } 0\le R<1\\ 1, \text{otherwise}\end{cases}$, $V=\sqrt{U_{p,q}^2+W_{p,q}^2}=\rho k\sqrt{n_{co}^2-n_{cl}^2}$. Now, by multiplying (A3) with $F_{lq}(R)$ and (A4) with $F_{lp}(R)$ and subtracting one from the other, we get

$$\left\{F_{lq}(R)R\frac{dF_{lp}(R)}{dR}\right\}_0^{\infty}-\left\{F_{lp}(R)R\frac{dF_{lq}(R)}{dR}\right\}_0^{\infty}=\left(U_q^2-U_p^2\right)\int_0^{\infty}F_{lp}(R)F_{lq}(R)RdR. \tag{A5}$$

From (6), the left-hand side of (A5) is zero. Hence, the inner product is nonzero if p is different from q, and otherwise zero. On the other hand, the maximality is trivial when we recall that F_{lp}'s are all the possible solutions of the boundary condition in (7). Hence, the orthogonality and maximality are completely proved.

B. Retrieval of mutual intensity profile

For retrieval of the mutual intensity profile, we use the method proposed by Rayman et. al. in ref. 17. The method uses Wigner function transform property through two cylindrical lenses and Radon transformation to retrieve the mutual intensity profile. While the method was proposed to retrieve an image, we adopt only a part of the proposed method – the retrieval of the mutual intensity profile. From now on, we closely follow the description in ref. 17.

The Wigner function is defined as follows[19]:

$$W(x,k_x,y,k_y)=\frac{1}{\pi^2}\int_{-\infty}^{\infty}\int_{-\infty}^{\infty}\exp[-2i(k_x\Delta x+k_y\Delta y)]\,\tilde{\Gamma}(x,y;\Delta x,\Delta y)\,d\Delta x\,d\Delta y\,, \tag{B1}$$

where $\tilde{\Gamma}$ is deduced from the mutual intensity profile Γ as

$$\tilde{\Gamma}(x,y;\Delta x,\Delta y)=\Gamma(x+\Delta x,y+\Delta y;x-\Delta x,y-\Delta y)\,. \tag{B2}$$

Here each x,y,k_x,k_y is scaled with a common length x_0, hence, is dimensionless[15]. Next, it is shown that after two mutually perpendicular cylindrical lenses, this Wigner function is angularly transformed as follows[19].

$$W'(x_\theta,k_\theta;y_\phi,k_\phi)=W(x,k_x;y,k_y), \tag{B3}$$

where

$$\begin{bmatrix}x_\theta\\k_\theta\end{bmatrix}=\begin{bmatrix}\cos\theta & \sin\theta\\-\sin\theta & \cos\theta\end{bmatrix}\begin{bmatrix}x\\k_x\end{bmatrix},\ \begin{bmatrix}y_\phi\\k_\phi\end{bmatrix}=\begin{bmatrix}\cos\phi & \sin\phi\\-\sin\phi & \cos\phi\end{bmatrix}\begin{bmatrix}y\\k_y\end{bmatrix}. \tag{B4}$$

It is also noted that (B4) is based on the Fresnel integral from the $z=0$ plane to the $z=D$ plane after two cylindrical lenses, which relates the electric field distributions between those two planes according to[17]:

$$e(x,y;z=D)=\int_{-\infty}^{\infty}\int_{-\infty}^{\infty}C\exp\left[ik\left(\frac{xx'}{L_1}+\frac{yy'}{L_2}-\frac{(x')^2}{2R_1}-\frac{(y')^2}{2R_2}\right)\right]\tilde{e}(x,y)dx'dy', \tag{B5}$$

where C is an unimportant constant and,

$$\begin{aligned} R_i &= R_{i0} + d_i, \\ L_i &= (D - d_i)(1 + d_i / R_{i0}), \\ \frac{1}{R_{i0}} &= \frac{1}{D - d_i} - \frac{1}{f_i} \quad (i = 1,2). \end{aligned} \qquad \text{(B6)}$$

After two mutually perpendicular cylindrical lenses with curvature R_{10}, R_{20} and focal lengths f_1, f_2, respectively, the intensity profiles are detected using a CCD camera. The accuracy of the retrieval depends on the resolution and linearity of the CCD camera.

Now, we introduce the line projection $P_{\theta\phi}$ as follows

$$P_{\theta\phi}(x_\theta, y_\phi) = \int_{-\infty}^{\infty}\int_{-\infty}^{\infty} W'(x_\theta, k_\theta; y_\phi, k_\phi) dk_\theta dk_\phi . \qquad \text{(B7)}$$

The intensity profile at $z = D$, i.e., $|e(x, y; z = D)|^2$ can be expressed as follows[15].

$$|e(x, y; z = D)|^2 = P_{\theta\phi}((\tilde{\beta} \sin\theta / L_1)x, (\tilde{\beta} \sin\phi / L_2)y), \qquad \text{(B8)}$$

where the angles θ, ϕ are related as

$$\theta = -\tan^{-1}(R_1 / \tilde{\beta}), \quad \phi = -\tan^{-1}(R_2 / \tilde{\beta}), \qquad \text{(B9)}$$

The inverse process to get $W(x, k_x; y, k_y)$ from $P_{\theta\phi}(x_\theta, y_\phi)$ is called the inverse Radon transform. It is noted that for successful inverse transformation, the angles θ, ϕ should be equally distributed in the interval $[0, \pi]$[17]. The number of necessary angles for satisfactory exactness of retrieval depends on the complexity of the Wigner function[17]. The more angles are used, the more exact results one can get.

The inverse Radon transform to get the Wigner function from intensity images consists of two distinct procedures, say, inverse Radon transform of the x,k_x pairs, and then the y,k_y pairs. Because these procedures are mutually independent from each other, we can consider only one of the two pairs independently at a time without loss of generality.

Now consider an arbitrary function $\psi(x_1,x_2)$ in the L_2 functional space. The Radon transform is defined by

$$\Re[\psi](x,\theta)=\int_{-\infty}^{\infty}\psi(x\cos\theta-u\sin\theta,x\sin\theta+u\cos\theta)du\,, \tag{B10}$$

The Radon transform is a line projection for a given angle θ, the line of which is parallel to a line through the origin with angle θ from the reference axis, say, X-axis and x is the distance between two lines. The inverse Radon transform is carried out with Fourier transform as follows.

$$\begin{aligned}M_F(\varpi,\theta)&\overset{\Delta}{=}F\{\Re[\psi](x,\theta)\}_x=\int_{-\infty}^{\infty}\Re[\psi](x,\theta)\exp[-i\varpi x]dx\\&=\int_{-\infty}^{\infty}\int_{-\infty}^{\infty}\psi(x\cos\theta-u\sin\theta,x\sin\theta+u\cos\theta)\exp[-i\varpi x]dudx\end{aligned}\,. \tag{B11}$$

Inducing new variable as

$$\begin{bmatrix}x_1\\x_2\end{bmatrix}=\begin{bmatrix}\cos\theta & -\sin\theta\\ \sin\theta & \cos\theta\end{bmatrix}\begin{bmatrix}x\\u\end{bmatrix},\ \begin{bmatrix}\zeta\\ \xi\end{bmatrix}=\begin{bmatrix}\varpi\cos\theta\\ \varpi\sin\theta\end{bmatrix}, \tag{B12}$$

gives

$$M_F(\zeta,\xi)=\int_{-\infty}^{\infty}\int_{-\infty}^{\infty}\psi(x_1,x_2)\exp[-i\zeta x_1-i\xi x_2]dx_1dx_2=F_2[\psi(x_1,x_2)]_{x_1,x_2}\,. \tag{B13}$$

Hence, to get $\psi(x_1, x_2)$, we need to solve the inverse 2-D Fourier transform as follows.

$$\begin{aligned}\psi(x_1, x_2) &= F_2^{-1}[M_F(\zeta,\xi)]_{\zeta,\xi} = \frac{1}{4\pi^2}\int_{-\infty}^{\infty}\int_{-\infty}^{\infty} M_F(\zeta,\xi)\exp[i\zeta x_1 + i\xi x_2]d\zeta d\xi \\ &= \frac{1}{4\pi^2}\int_0^{2\pi}\int_{-\infty}^{\infty} M_F(\nu,\varphi)\exp[i\nu(x_1\sin\varphi + x_2\cos\varphi]|\nu|d\zeta d\xi\end{aligned}, \qquad \text{(B14)}$$

where we changed the integral variables. In practice, the integration for the angle ν is carried out as a summation of a number of data sets.

References

1. E. Snitzer, H. Po, F. Hakimi, R. Tumminelli, and B. C. McCollum, "Double-clad, offset core Nd fiber laser," in Proceedings of Conference on Optical Fiber Sensors, Postdeadline paper PD5, 1988.
2. L. Zenteno, "High-power double-clad fiber lasers," J. Lightwave Technol. **11**, 1435-1446 (1993).
3. T. Weber, W. Luthy, H. P. Weber, V. Neuman, H. Berthou, G. Kotrotsios, J. P. Dan, and H. E. Hintermann, "Cladding-pumped fiber laser," IEEE J. Quantum Electron. **31**, 326-329 (1995).
4. O. G. Leminger and G. K. Grau, "Nearfield-intensity and modal power distribution in multimode graded-index fibres," Electron. Lett. **16**, 678-679 (1980).
5. G. K. Grau and O. G. Leminger, "Relations between near-field and far-field intensities, radiance and modal power distribution of multimode graded-index fibres," Appl. Opt. **20**, 457-459 (1981).
6. A. R. Mickelson, M. Eriksrud, S. Aamlid, and N. Ryen, "Role of the fusion splice in the concatenation problem," J. Lightwave Technol. **LT-2**, 126-138 (1984).
7. A. R. Mickelson and M. Eriksrud, "Mode-continuum approximation in optical fibers," Bell Syst. Tech. J. **52**, 1563-1578 (1973).
8. D. Rittich, "Practicability of determining the modal power distribution by measured near and far fields," J. Lightwave Tech. **LT-3** (3), 652-661 (1985).
9. F. Gori, M. Santarsiero, R. Borghi, G. Guattari, "Intensity-based modal analysis of partially coherent beams with Hermite-Gaussian modes," Opt. Lett. **23** (13), 989-991 (1998).

10. F. Gori, M. Santarsiero, R. Simon, G. Piquero, R. Borghi, G. Guattari, "Coherent-mode decomposition of partially polarized, partially coherent sources," J. Opt. Soc. Am. A **20** (1), 78-84 (2003).

11. C. Elster, I. Weingartner, "Solution to the shearing problem," Appl. Opt. **38** (23), 5024-5031 (1999)

12. E. L. Lago, R. de la Fuente, "Wavefront sensing by diffracted beam interferometry," J. Opt. A.-Pure Appl. Opt. **4** (3), 299-302 (2002).

13. G. Z. Yang, B. Z. Dong, B. Y. Gu, J. Y. Zhuang, O. K. Ersory, "Gerchberg-Saxton and Yang-Gu algorithms for phase retrieval in a nonunitary transform system – a comparison," Appl. Opt. **33** (2), 209-218 (1994).

14. W. Snyder and J. D. Love, *Optical waveguide theory* (Kluwer academic publishers, Massachusetts, USA, 1983).

15. J. W. Goodman, *Introduction to Fourier optics*, (McGraw-Hill, New York, USA, 1968).

16. K. A. Nugent, "Wave field determination using three-dimensional intensity information," Phys. Rev. Lett. **68** (15), 2261-2264 (1992).

17. M. G. Raymer, M. Beck, and D. F. McAlister, "Complex wave-field reconstruction using phase-space tomography," Phys. Rev. Lett. **72** (8), 1137-1140 (1994).

18. D. F. McAlister, M. Beck, L. Clarke, A. Mayer, and M. G. Raymer, "Optical phase retrieval by phase-space tomography and fractional-order Fourier transforms," Opt. Lett. **20** (10), 1181-1183 (1995).

19. J. Tu and S. Tamura, "Wave field determination using tomography of the ambiguity function," Phys. Rev. E, **55** (2), 1946-1949 (1997).

20. J. Bertrand and P. Bertrand, “A tomographic approach to Wigner function,” Found. Phys. **17** (4), 397-405 (1987).

Table

Modes	Effective Index	Test Modal Weight $|c_i|^2$	Calculated Results			
			Simulation A $|c_i|^2$	Error (%)	Simulation B $|c_i|^2$	Error (%)
LP01 cos	1.4686	64	64.03	0.05	60.39	5.64
LP02 cos	1.4604	25	24.90	0.40	27.45	9.80
LP11 cos	1.4655	4	3.988	0.30	4.391	9.78
LP11 sin	1.4655	9	9.045	0.50	9.829	9.21
LP21 cos	1.4615	1	1.003	0.30	1.100	10.0
LP21 sin	1.4615	9	9.027	0.30	8.630	4.11
LP31 cos	1.4570	4	3.981	0.48	4.241	6.01
LP31 sin	1.4570	1	1.002	0.20	0.910	9.00

Table 1. The table lists the modes of the step-index fiber considered in the simulations and their effective indices. For the numerical verification of our method, each mode was excited with a power represented by the test modal weight. This was then retrieved with two different simulation procedures, A and B, with the results shown in the table.

Figure Captions

Fig. 1. Measurement setup for determination of the mutual intensity profile

Fig. 2. The calculated intensity distribution of each mode: (a) the modal solutions inside fiber, (b) the modal solutions after the spherical lens

Fig. 3. A test multimode beam with arbitrary assigned initial modal power: (a) the beam intensity inside fiber, (b) the free space beam intensity at $z = f$.

Fig. 4. Selected CCD images for different θ, ϕ, i.e., with different positions of the lenses and the CCD array.

Fig. 5. Comparison between the test multimode beam and reconstructed beam from calculated results. The figure shows the intensity pattern of the test multimode beam inside the fiber (solid line), the reconstructed image from simulation A (dashed line), and the reconstructed image from simulation B (dotted line). Fig 5(b) is a magnified portion of Fig 5(a) to clarify the small differences between results.

Fig. 6. The modal power distribution among modes. The test modal power distribution, and the results with simulations A and B are shown.

Figures

Fig. 1

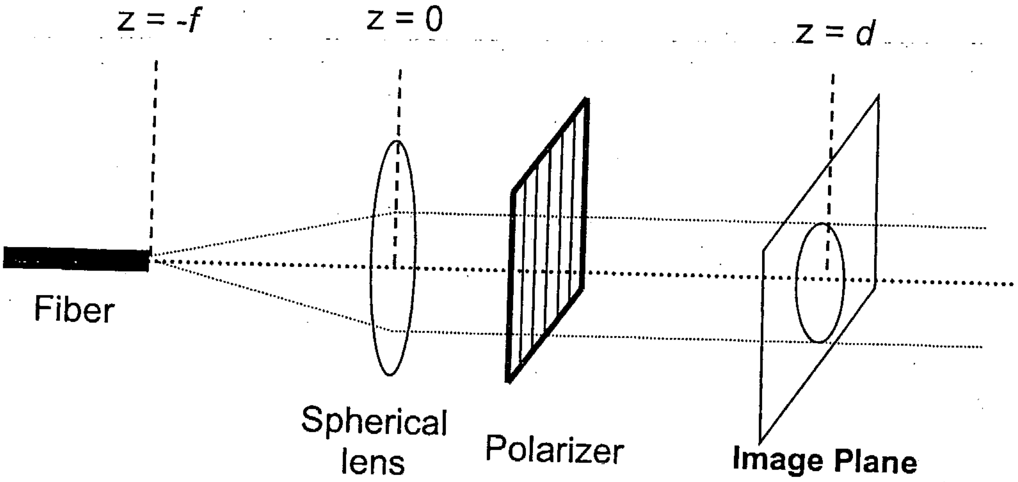

Fig. 2

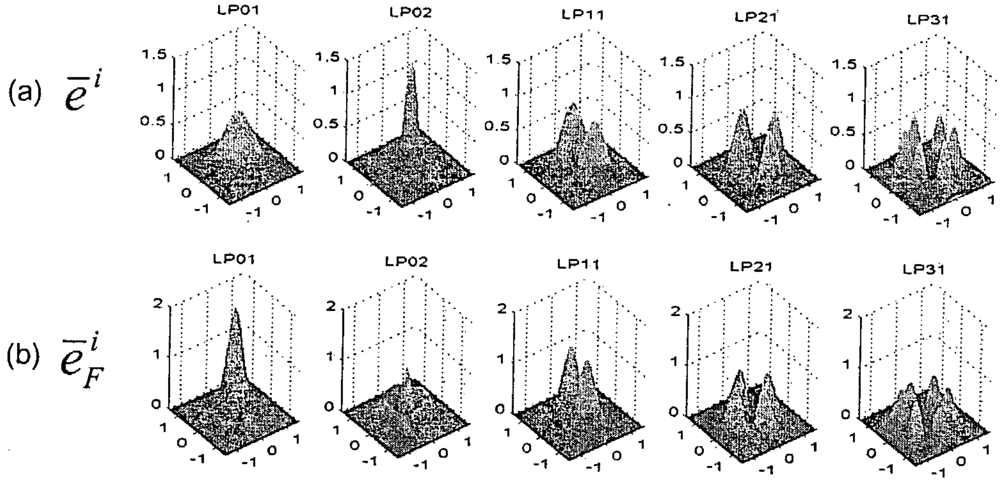

Fig. 3

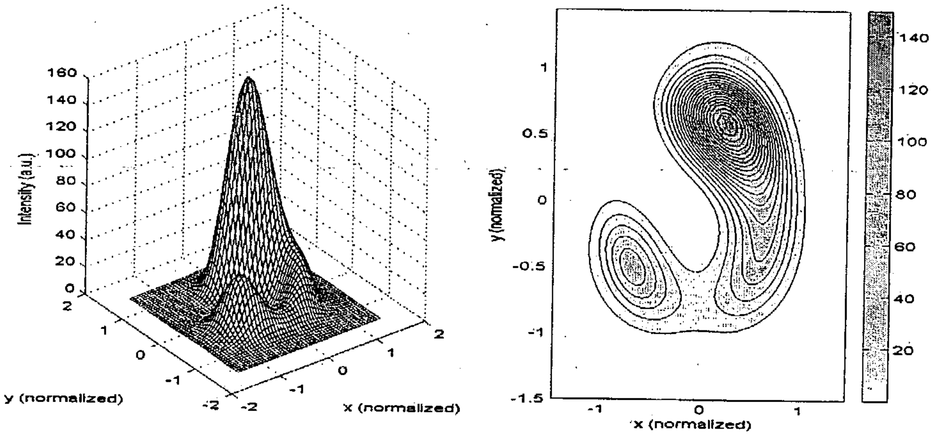

(a) $e(x, y; z = -f)$

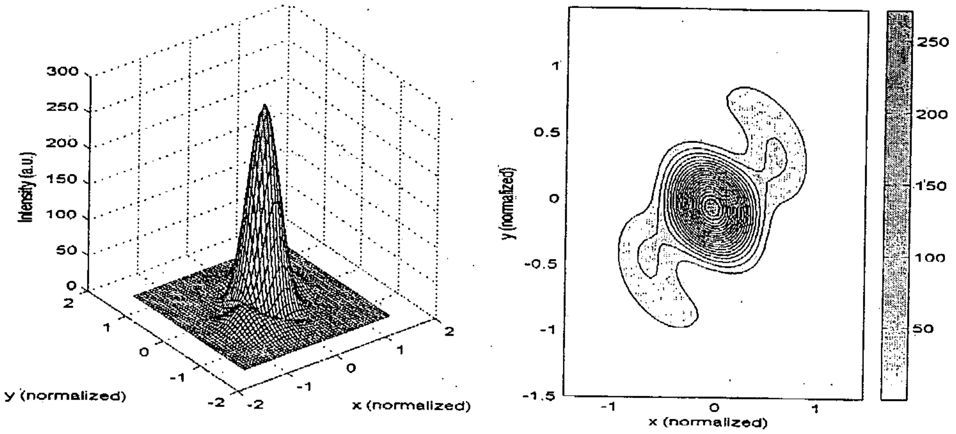

(b) $e(x, y; z = f)$

Fig. 4

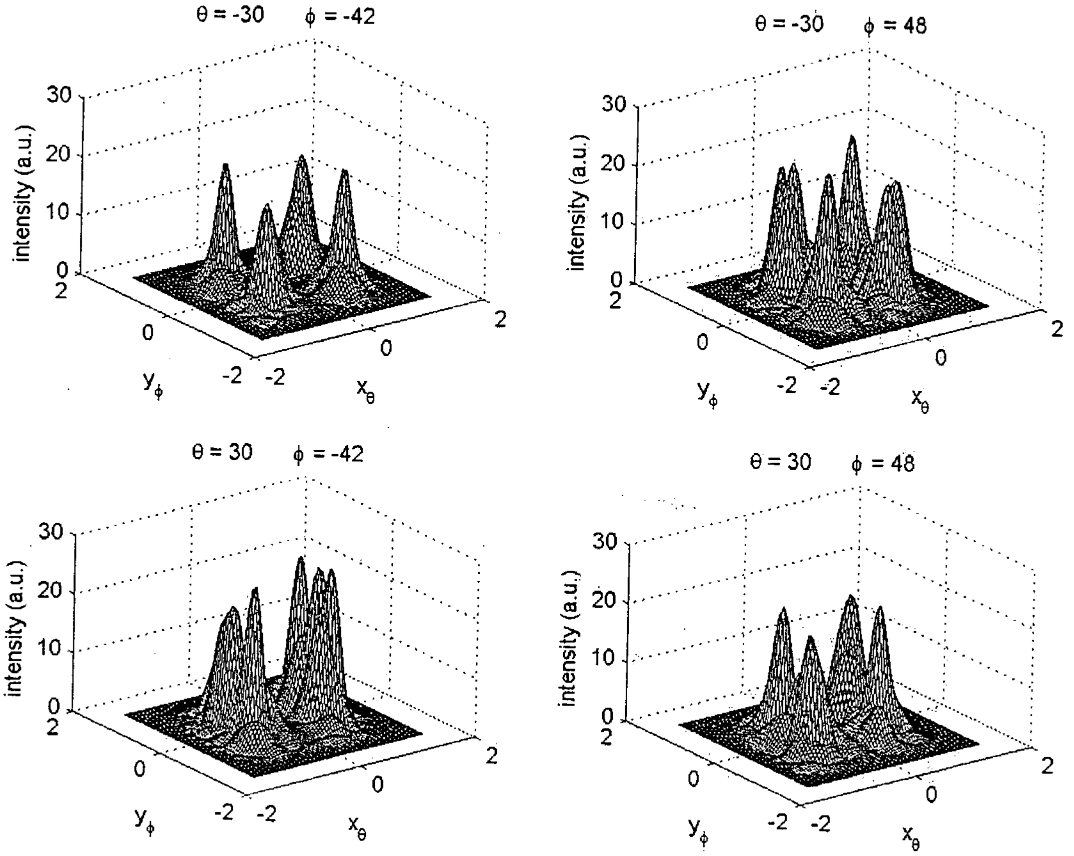
θ = -30 ϕ = -42
θ = -30 ϕ = 48
θ = 30 ϕ = -42
θ = 30 ϕ = 48
intensity (a.u.)
30
20
10
0
2
0
-2
-2
0
2
y_ϕ
x_θ

Fig. 5

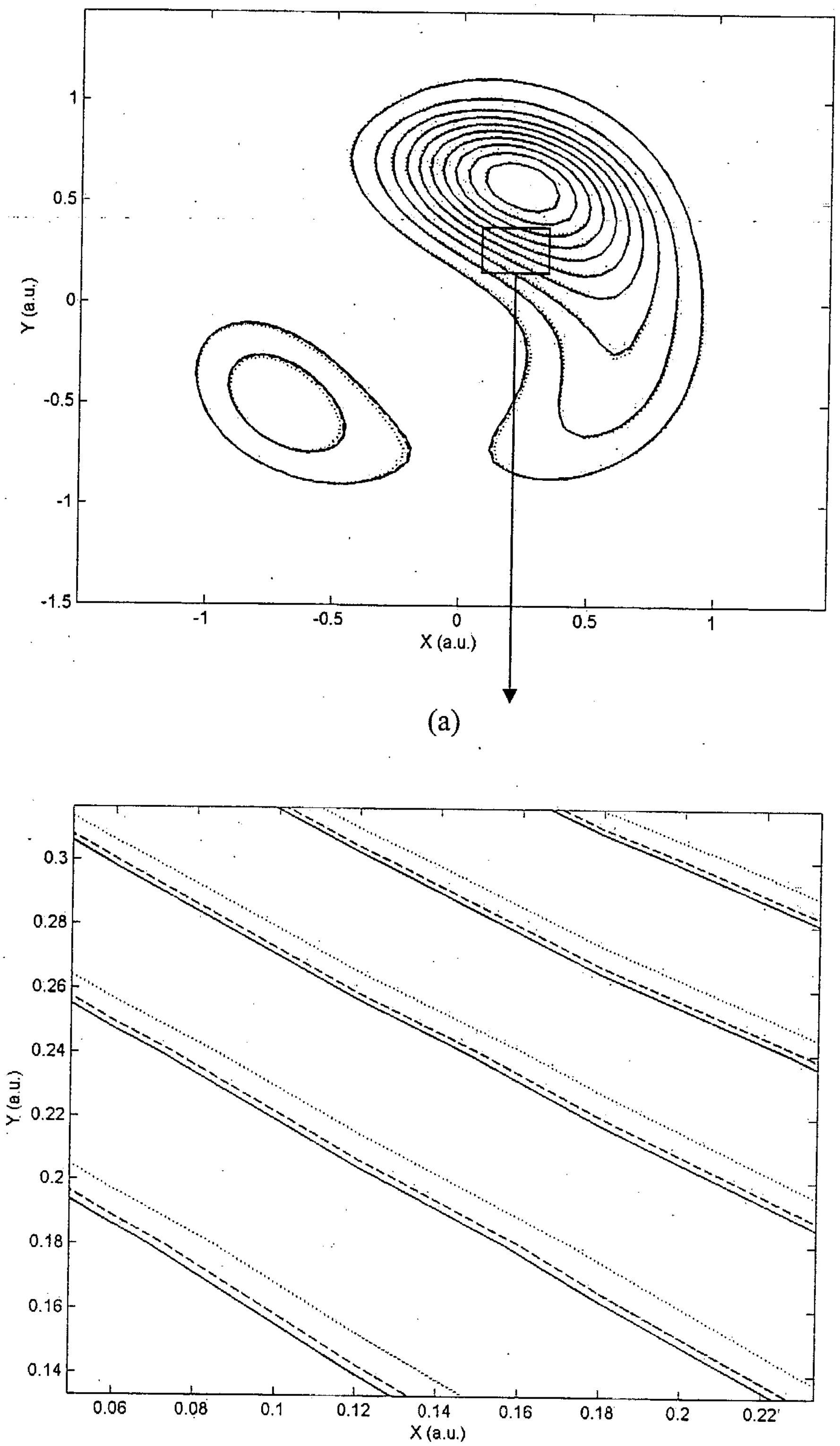
Y (a.u.)
1
0.5
0
-0.5
-1
-1.5
-1
-0.5
0
0.5
1
X (a.u.)
Y (a.u.)
0.3
0.28
0.26
0.24
0.22
0.2
0.18
0.16
0.14
0.06
0.08
0.1
0.12
0.14
0.16
0.18
0.2
0.22
X (a.u.)

(a)

(b)

Fig. 6

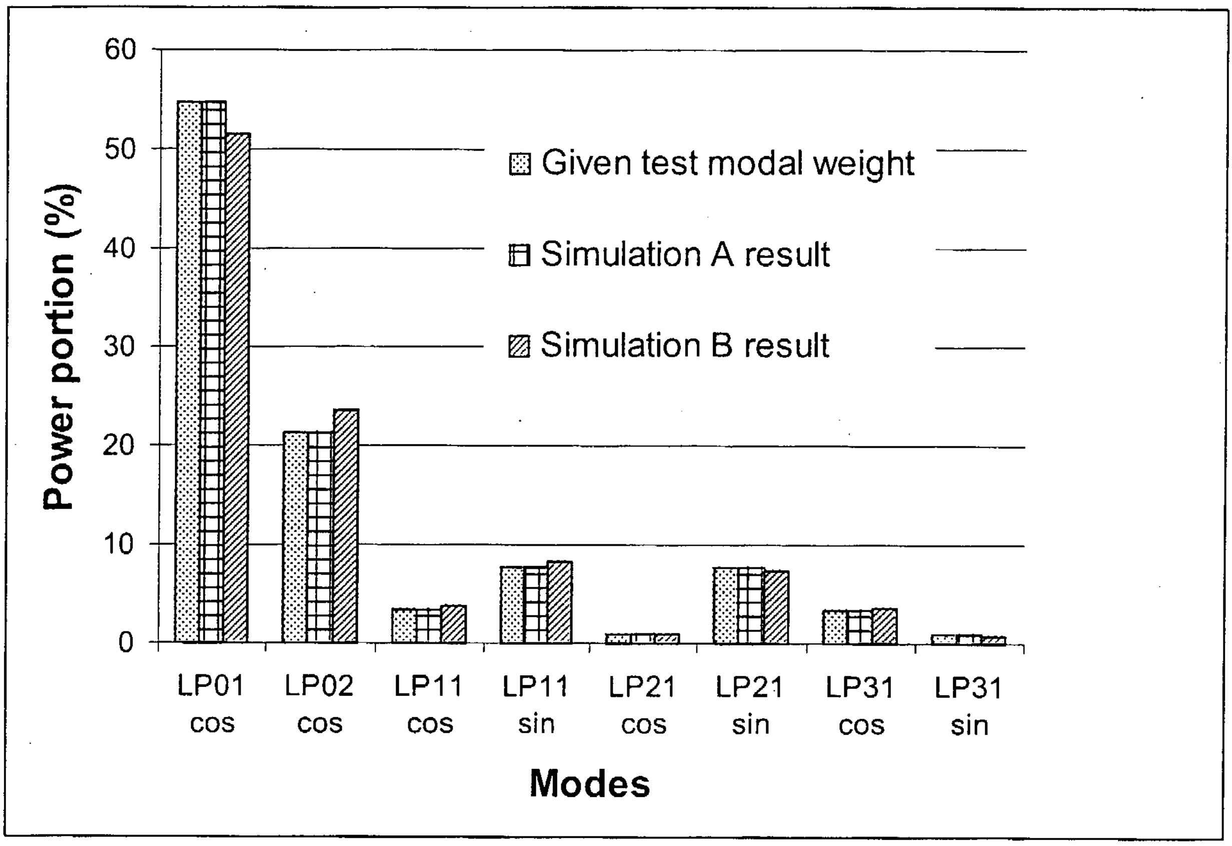
60
50
40
30
20
10
0
Power portion (%)
Given test modal weight
Simulation A result
Simulation B result
LP01 cos
LP02 cos
LP11 cos
LP11 sin
LP21 cos
LP21 sin
LP31 cos
LP31 sin
Modes